Applied Catalysis B: Environmental 160–161 (2014) 179–187

Contents lists available at ScienceDirect

Applied Catalysis B: Environmental

journal homepage: www.elsevier.com/locate/apcatb

Efficient electrochemical reduction of bromate by a Pd/rGO/CFP electrode with low applied potentials

Ran Mao [a,b], Xu Zhao [a,*], Huachun Lan [a], Huijuan Liu [a], Jiuhui Qu [a]

[a] Key Laboratory of Aquatic Science and Technology, Research Center for Eco-Environmental Sciences, Chinese Academy of Sciences, Beijing 100085, PR China

[b] University of Chinese Academy of Sciences, Beijing 100049, PR China

ARTICLE INFO

Article history:
Received 26 December 2013
Received in revised form 5 April 2014
Accepted 23 April 2014
Available online 4 May 2014

Keywords:
Electrochemical reduction
Bromate removal
Pd/rGO/CFP electrode
Low applied potential

ABSTRACT

The reduced graphene oxide/carbon fiber paper (rGO/CFP) composites are synthesized by in situ chemical reduction method, and then Pd nanoparticles are supported on the rGO/CFP via an electrodeposition process to obtain a novel Pd/rGO/CFP cathode, which is used for bromate (BrO_3^-) electroreduction. Pd particles are fairly well dispersed on the rGO nanosheets with a mean size of 6.7 nm. With the Pd/rGO/CFP electrode, the removal efficiency of BrO_3^- is up to 98.7% within 60 min at −0.5 V; the BrO_3^- reduction follows pseudo-first-order kinetics with the rate constant of 0.105 min^{-1}, which is much higher than that of CFP, Pd/CFP or rGO/CFP electrode. The rate constant is largely increased from 0.001 to 0.105 min^{-1} upon lowering the cathode potential from 0 to −0.5 V, and is slightly decreased at more negative potentials. At −0.5 V, the reduction rate is significantly enhanced at low pH, while at −1.5 V, the pH effect is reduced. Within the concentration of GO precursor from 0.5 to 2.0 mg/mL, the as-prepared Pd/rGO/CFP electrode exhibits high and stable electrocatalytic activity. The rGO sheets shorten the effective lengths for electron transfer in the electroreduction of H_2O/H^+ to produce atomic H* for the indirect reduction of BrO_3^- to Br^-. Accordingly, a high removal efficiency can be achieved with the applied potential as low as −0.5 V, which is less negative than that for H_2 evolution. Due to the strong interaction between surface oxides of rGO and Pd, the high stability of the composite film electrode is exhibited.

1. Introduction

Bromate (BrO_3^-) is an oxyhalide disinfection byproduct frequently detected in drinking water from ozonation or chlorination of bromide (Br^-)-containing source waters, and has been recognized as a potential carcinogen to humans [1]. Various kinds of methods have been developed to eliminate BrO_3^- ions in water, including filtration, chemical reduction, activated carbon techniques, and biological remediation [2–5]. However, second pollution and high consumption of reagents are inevitable in the removal process [6]. Electrochemical transformation process, particularly electroreduction process, has successfully been applied for dechlorination of chloroorganics and elimination of nitrate ions in water due to its environmental compatibility and selectivity [7–9]. Thus, the electrochemical reductive treatment can be a promising method for eliminating BrO_3^- ions because it requires only electricity in operation, and no second pollution companied [10–13]. BrO_3^- can be transformed to nontoxic Br^- by the reduction at the cathode.

It is recognized that the reduction of contaminants at cathode surfaces may occur through both direct and indirect mechanisms [14]. Direct reduction of contaminants at the cathode requires suitable electrode materials, which usually work at high overpotentials to obtain vigorous reduction conditions [15]. Indirect electroreduction occurs via the surface-adsorbed atomic H*, a highly activated intermediate hydrogen radical produced from water reduction [16]. As demonstrated by many researchers, Pd has the unique property of activating H_2 as well as catalyzing the electrochemical reduction of H_2O/H^+ to produce continuously adsorbed nascent H* [17]. The Pd—H bonds are based on multiple σ-bonding between the hydrogen atoms and the d orbitals of the Pd atoms [18]. Although the Pd-catalytic electroreduction has been well reported, the enhancement of reaction rates was not obvious until the cathode potential was more negative than that for H_2 evolution, due to that H_2 was the major source for atomic H* [8,9,15,19]. As a result, the vigorous H_2 bubbles at the cathode surface would

* Corresponding author. Tel.: +86 10 62849160; fax: +86 10 62849160.
E-mail address: zhaoxu@rcees.ac.cn (X. Zhao).

http://dx.doi.org/10.1016/j.apcatb.2014.04.040
0926-3373/

inevitably deactivate the Pd-modified electrodes. Therefore, it is highly desirable to develop a novel Pd-loaded electrode to decrease the potential for atomic H* generation.

Recently, the emergence of graphene has turned on a novel insight for applying two-dimensional carbon material as support for catalyst nanoparticles due to its high specific surface area and sufficient electrical conductivity [20–23]. Hybridization of metal catalysts with graphene has been reported in order to achieve cost-effective electrodes in solar cells, and it is found to provide promising results [24,25]. Previous reports on graphene-supported Pd nanoparticles, however, mainly focused on the applications for electrochemical capacitors or fuel cells [26–28]. To the best of our knowledge, the environmental applications of the graphene/Pd deposited electrodes for contaminants electroreduction have not been studied so far.

Carbon fiber paper (CFP) was used as the substrate material due to its low electrical resistivity, minimal electrochemical corrosion and good handling. On the CFP substrate, reduced graphene oxide (rGO) can be cheaply produced on a large scale from graphene oxide (GO) [29]. The existence of rGO can result in the increase in the electronic mobility and thereby the enhancement in electroreduction performance due to its unique properties [23,28]. In contrast, Pd nanoparticles could be easily deposited on the surface of rGO based on oxygen-containing groups [26,27]. Thus, combination of Pd nanoparticles and rGO sheets as a composite film is expected to increase the catalytic activity for electrochemical reduction of BrO_3^-, and also inhibit the H_2 evolution reaction efficiently.

In the present work, a facile and effective two-step approach for fabricating the rGO based carbon materials as Pd electrocatalyst support for BrO_3^- reduction has been proposed. The obtained results shed some light on how rGO sheets on CFP electrode benefit the Pd-catalytic electroreduction of contaminants with a low applied cathode potential, thus providing an alternative to both inhibit the negative effect of vigorous H_2 bubbles on the electrochemical reaction and reduce the energy consumption for H_2 evolution.

2. Experimental

2.1. Chemicals

GO dispersion was obtained from Nanjing XFNano Materials Tech Co., Ltd. The CFP substrate was purchased from Beijing LN Power Source Company (TGP-H-090, Toray). Proton exchange membrane employed in the experiments was Nafion-117 (Du Pont). Other chemicals including ascorbic acid (VC), sodium bromate, sodium bromide, palladium chloride ($PdCl_2$) and ammonium chloride (NH_4Cl) were purchased from Sinopharm Chemical Reagent Co. Ltd., with their purity in analytical grade. pH regulation was performed using either NaOH or H_2SO_4 (guaranteed grade). All the aqueous solutions were prepared with Millipore water having a resistivity of 18.2 MΩ.

2.2. Fabrication of the Pd/rGO/CFP cathode

The Pd/rGO/CFP electrode was prepared through in situ chemical reduction of the GO film on the CFP substrate using VC as the reducing agent, followed by electrochemically depositing Pd on the rGO/CFP. The CFP substrate was made of carbon fibers having a diameter of approximately 8–10 μm. Prior to use, CFP was first immersed in a 0.1% (w/w) Triton X-100 solution for 24 h and then in deionized water for 2 h to lower the hydrophobicity and the extent of metal agglomeration. Then it was heated at 400 °C for 5 h to increase the surface oxygenated functional groups, and thereby increase the impregnation in GO dispersion. In a typical synthetic procedure for rGO/CFP, CFP (25 mm × 50 mm × 0.28 mm, bulk density 0.44 g/cm^3) was immersed in a GO suspension (0.5, 1.0, 1.5 or 2.0 mg/mL). GO films were formed on the CFP by sonicating the system under ambient temperature for ca. 5 h. Subsequently, the GO film coated CFP was transferred to plastic tubes (diameter 3.0 cm) containing 30.0 mL of 10.0 mg/mL VC. The reaction system was allowed to remain undisturbed overnight and then heated at 60 °C for 2 h. After repeatedly rinsed with deionized water, a uniform rGO coated CFP was obtained and was used for depositing Pd nanoparticles via our previously reported electrodeposition method [19]. In brief, the Pd nanoparticles were electrodeposited on the rGO/CFP electrode from aqueous solutions of 10 mM NH_4Cl containing 1 mM $PdCl_2$ (pH = 1) as precursor at a constant current of 0.02 A for 10 min. For comparative purposes, a sample of Pd-loaded CFP was also prepared under the same conditions.

2.3. Apparatus

All electrochemical experiments were performed with an EG&G model 263A workstation (Princeton Applied Research, USA). A conventional three-electrode system batch reactor with an effective volume of 100 mL was employed, which was separated into cathode cell (50 mL) and anode cell (50 mL) by the proton exchange membrane. The as-prepared electrodes with a geometric surface area of 7.5 cm^2 (2.5 cm × 3 cm) served as the working electrode. A platinum wire with 72 mm in length and 1.5 mm in diameter was used as the counter electrode, and a saturated calomel electrode (SCE) was employed as the reference electrode. To ensure the homogeneity of the catholyte, the system was magnetically stirred at a rate of 700 rpm. The potentiostatic electrolysis was applied throughout the BrO_3^- reduction experiments with 2 mM Na_2SO_4 as the background electrolyte. During the electrolysis, samples were periodically withdrawn from the cathode cell for analysis.

2.4. Analytical method

The concentration of $Pd^{2\pm}$ in the electrolyte before and after the electrodeposition was measured by the inductively coupled plasma optical emission spectrometer (ICP-OES, PerkinElmer Co.) to quantify the Pd loading amount on the Pd-loaded electrodes. The concentrations of BrO_3^- and Br^- were measured using ion chromatograph (IC, ICS-2000, Dionex, Sunnyvale, CA) equipped with an IonPac AS-19 anion column and an IonPac AG19 guard column. Mobile phase eluent for the IC was KOH solution, and the flow rate was 1.0 mL/min. The chromatogram of BrO_3^- and Br^- was obtained under gradient elution conditions (0.0–18.0 min, 10.0 mM KOH; 18.1–26.0 min, 35.0 mM KOH; and 26.1–31.0 min, 10.0 mM KOH). The pH was measured using a 9165 BN pH electrode connected to an Orion-828 pH analyzer (Orion Research, Inc., Beverly, MA).

The morphology of the cathodes was characterized using JSM 6301 scanning electron microscopy (SEM). X-ray powder diffraction (XRD) patterns of the samples were obtained with an X'Pert PRO Powder diffractometer machine (PANalytical Co.), by using Ni-filtered Cu K_α radiation from 5° to 90° (in 2θ). Raman spectra were recorded on a Bruker Senterra Raman spectrometer and microscope through a 20× objective lens using a 20 mW and a 514 nm laser excitation. X-ray photoelectron spectroscopy (XPS) analysis was carried out with an ESCALAB 250 photoelectron spectrometer (ThermoFisher Scientific, USA). Cyclic voltammetry (CV) analysis was also performed in the EG&G model 263A workstation. Electrochemical impedance spectra (EIS) were recorded in the potentiostatic mode. The amplitude of the sinusoidal wave was

10 mV, and the frequency of the sinusoidal wave was in the range from 0.1 Hz to 100 kHz.

3. Results and discussion

3.1. Characterization of the electrodes

The as-synthesized rGO/CFP, Pd/CFP and Pd/rGO/CFP electrodes are firstly characterized by SEM analysis. The rGO nanosheets formed on the carbon fibers appear like a flexible thin film with a number of wrinkles (Fig. 1a), generating an sp^2 atomic carbon network. On the Pd/CFP, abundant sphere-like Pd nanoparticles are uniformly deposited on the carbon fibers with an average size of around 20 nm (Fig. 1b). In the case of the Pd/rGO/CFP, the rGO sheets providing a substrate for depositing Pd particles had promoted particle agglomeration and growth (Fig. 1c), presumably owing to a strong interaction between residual surface oxides (e.g., carbonyl groups) and Pd ions. XRD patterns of the Pd/CFP and Pd/rGO/CFP electrodes are recorded in Fig. 1d, where diffraction peaks assigned to (1 1 1), (2 0 0), (2 2 0) and (3 1 1) of metallic Pd are observed. The primary Pd crystallite size of the Pd/CFP and Pd/rGO/CFP electrode is calculated to be 12.9 and 6.7 nm by Scherrer's formula, respectively. It was noticed that the XRD method gives the mean size of the crystallites, rather than the size of the particles, which are aggregated primary particles/crystallites [30]. Hence, the particle size showed by the SEM images is larger than the primary crystallite size.

The chemical structure of the electrodes is furthermore studied. It is found that after the reduction process the absorbance peak at 284.8 eV (C—C) becomes predominant while the additional peaks of oxygen functionalities at 286.8 eV (C—O) and 289.8 eV (O—C=O) are obviously reduced (Fig. 2a and b), suggesting that most oxygen-containing functional groups of GO were successfully removed by VC. Fig. 2d and e clearly shows the two peaks centered at 335.0 and 340.3 eV, which can be assigned to Pd $3d_{5/2}$ and Pd $3d_{3/2}$ of Pd^0 metal, respectively. In comparison with the Pd/CFP, the two intensified peaks centered at 336.6 and 341.8 eV are characteristics of so-called "electro-deficient" Pd species, indicating the formation of PdO_x on the Pd/rGO/CFP [26]. Meantime, the oxygenated functional groups on the rGO surface are further reduced after the electrodeposition of Pd nanoparticles (Fig. 2c). In the Raman spectrum of GO/CFP, rGO/CFP and Pd/rGO/CFP electrodes, the two prominent bands around 1350 cm^{-1} and 1580 cm^{-1} are assigned to the D and G bands of carbon, respectively (Fig. 2f). The I_D/I_G value of the Pd/rGO/CFP was calculated to be 1.39, higher than that of GO/CFP (0.75) and rGO/CFP (1.15). This result indicates the small size of the in-plane sp^2 domains of rGO [31,32]. And, Pd nanoparticles may induce defects and structural disorder within the synthesized rGO sheets [26].

On the basis of the above results, it can be inferred that the rGO may play an important part in the formation of Pd nanoparticles. The rGO sheets prepared through the chemical reduction leave behind some defects and vacancies, which can act as good anchoring sites for the deposition of metal nanoparticles. The well-dispersive Pd with a small primary crystallite size can be ascribed to the redox reaction between residual oxygen related species on rGO and Pd ions, which is similar to the reaction mechanism between Pt nanoparticles and single-walled carbon

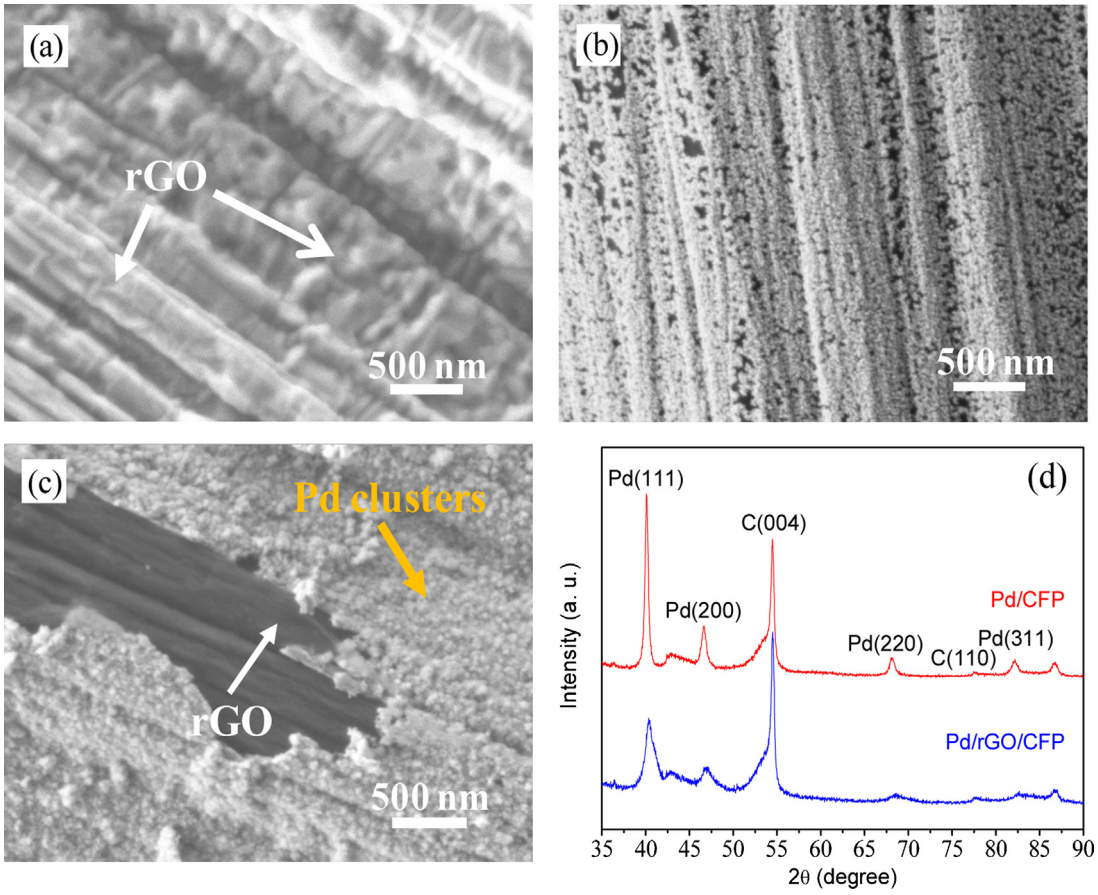

Fig. 1. SEM images of (a) rGO/CFP, (b) Pd/CFP, and (c) Pd/rGO/CFP. (d) XRD patterns of Pd/CFP and Pd/rGO/CFP.

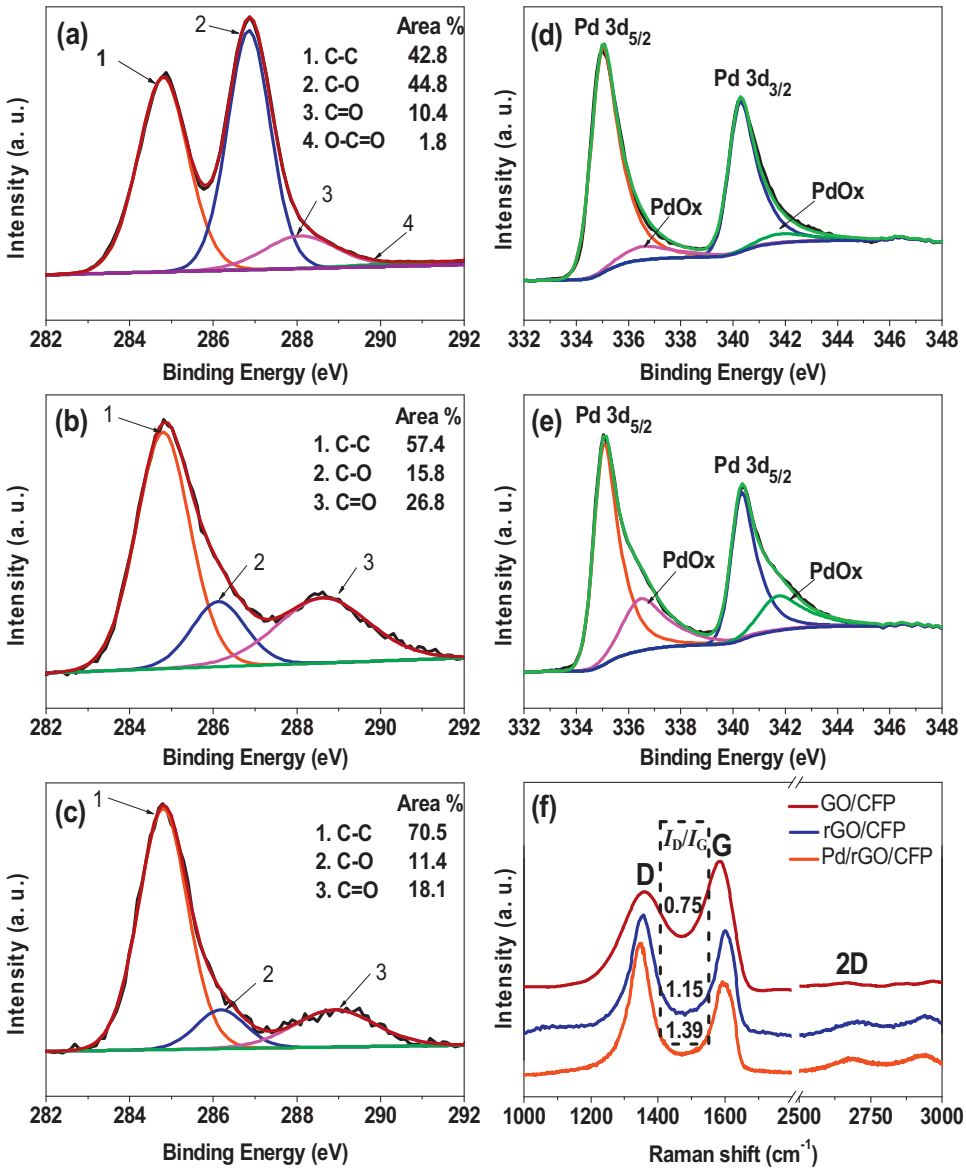

Fig. 2. XPS spectra of (a) C 1s of GO/CFP, (b) C 1s of rGO/CFP, (c) C 1s of Pd/rGO/CFP, (d) Pd 3d of Pd/CFP and (e) Pd 3d of Pd/rGO/CFP. (f) 514 nm excited Raman spectra of GO/CFP, rGO/CFP and Pd/rGO/CFP electrodes.

nanotubes proposed by Choi et al. [33]. The Pd loading amount on either Pd/CFP or Pd/rGO/CFP electrode is determined to be 0.42 mg/cm^2 as measured by the ICP-OES.

3.2. Performance of the Pd/rGO/CFP electrode for BrO_3^- reduction

The BrO_3^- electroreduction and corresponding Br^- formation on different cathodes (CFP, Pd/CFP, rGO/CFP, and Pd/rGO/CFP) are compared at −0.5, −1.0, −1.5 and −2.0 V (Fig. 3a and Fig. S1). At −0.5 V, up to 98.7% of BrO_3^- is reduced at the Pd/rGO/CFP electrode within 60 min, while only 3.4%, 59.9% and 32.9% of BrO_3^- is transformed at the CFP, Pd/CFP and rGO/CFP electrode, respectively. Under the tested conditions, the sum of BrO_3^- and Br^- accounts for more than 92% of bromine balance with all the electrodes, indicating the quantitative transformation of BrO_3^- to Br^-. The average missing 8% for bromine mass balance suggests that other bromine species such as BrO_2, $HBrO_2$ and $HOBr/OBr^-$ are formed in the reduction process. $HOBr/OBr^-$ are quantified as low as several ppb in all batch trials. The intermediates would undergo electrochemical reduction to produce Br_2 which must then be reduced to Br^- at the potential of the catalytic reduction, thus the final product of BrO_3^- reduction was Br^- [34].

Regarding the electrochemical reduction process, two mechanisms that have been proposed involve direct electron transfer and indirect reduction via atomic H* [35]. Direct reduction may occur by electron tunneling or by the formation of a chemisorption complex for target compounds with cathode materials [14]. Indirect reduction normally requires noble metal catalysts (e.g. Pd, Ag, and Ni) that convert H (from electroreduced H_2O/H^+ or/and H_2) into atomic H* [11,36,37]. On the surface of CFP and rGO/CFP electrodes, no atomic H* will be generated in the absence of metal catalysts [38]. Accordingly, the electroreduction of BrO_3^- is supposed to proceed via the direct mechanism on the CFP and rGO/CFP electrodes, and proceed with both direct electron transfer and indirect Pd-catalytic hydrodeoxygenation mechanism on the Pd/CFP and Pd/rGO/CFP electrodes. The higher activity exhibited by the rGO/CFP over the CFP electrode can be ascribed to the enhanced direct electron

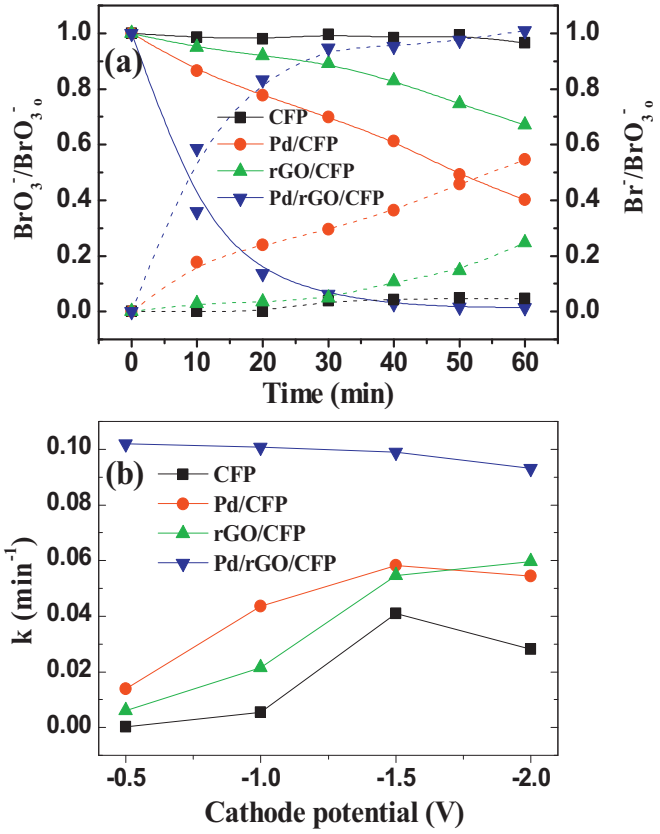

Fig. 3. (a) BrO_3^- removal (solid line) and Br^- formation (dashed line) at −0.5 V with CFP, Pd/CFP, rGO/CFP and Pd/rGO/CFP electrodes; (b) effect of cathode potential on BrO_3^- reduction kinetics with CFP, Pd/CFP, rGO/CFP and Pd/rGO/CFP electrodes (initial BrO_3^- concentration: 1 mg/L, 2 mM Na_2SO_4, GO = 1.5 mg/mL, pH = 6.03).

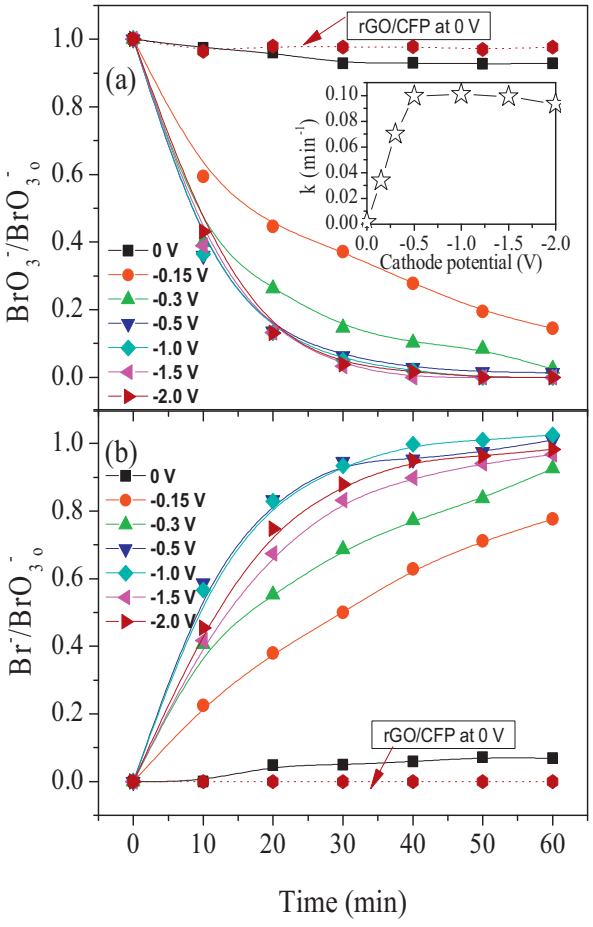

Fig. 4. Effect of cathode potential on (a) BrO_3^- reduction and (b) Br^- formation at the Pd/rGO/CFP electrode (initial BrO_3^- concentration: 1 mg/L, 2 mM Na_2SO_4, GO = 1.5 mg/mL, pH = 6.03).

transfer caused by the rGO sheets. The indirect reduction process efficiently proceeding on the Pd/CFP and Pd/rGO/CFP electrodes increased their catalytic activity for BrO_3^- reduction compared with the CFP and rGO/CFP electrodes.

The corresponding pseudo-first-order kinetic rate constants with different electrodes are shown in Fig. 3b. At −0.5 V, the rate constant of BrO_3^- reduction on the Pd/rGO/CFP electrode is 681.8, 7.2 and 16.5 times higher than that on the CFP, Pd/CFP and rGO/CFP electrode, respectively, coinciding with the electrocatalytic reduction performance. With decreasing the cathode potentials, the difference is reduced to some extent.

Considering that the difference of Pd surface morphology between the Pd/CFP and Pd/rGO/CFP electrodes might have affected the electroreduction of BrO_3^-, the comparative experiments are performed to clarify the surface morphology effect (Fig. S2). The Pd/GO/CFP electrode was prepared for the comparison with the same procedure for fabricating Pd/rGO/CFP, in which the only difference was that the chemical reduction of GO to rGO by ascorbic acid was not required. The SEM images and XRD patterns show that the as-prepared Pd/GO/CFP electrode (Pd loading amount 0.42 mg/cm^2) has a similar surface morphology with the Pd/rGO/CFP electrode in both particle agglomeration and primary Pd crystallite size. However, the elctrocatalytic activity of the Pd/GO/CFP electrode toward BrO_3^- reduction was determined to be much lower than that of the Pd/rGO/CFP electrode, indicating the surface morphology is not necessarily in correlation with the electrocatalytic activity. Thus, the higher elctrocatalytic activity of the Pd/rGO/CFP electrode over the Pd/CFP electrode can be ascribed to the rGO effect rather than the Pd surface morphology effect on the electroreduction.

3.3. *Effect of cathode potential*

The electrochemical reduction of BrO_3^- on the Pd/rGO/CFP electrode at different cathode potentials is investigated and the results are presented in Fig. 4. The rate constant largely increases from 0.001 up to 0.105 min^{-1} upon lowering the cathode potential from 0 to −0.5 V, and then reaches a plateau of around 0.010 min^{-1} at more negative potentials. From 0 to −0.5 V, although the decrease in cathode potentials can also enhance the direct reduction process, its contribution is minimal as minute BrO_3^- removal was achieved till the cathode potential was −0.5 V on the rGO/C electrode with direct mechanism. Hence, the indirect reduction process predominantly contributes to the significant BrO_3^- removal with the Pd/rGO/CFP electrode. It has been reported in many studies that the indirect reduction of contaminants happened at potentials more negative than −1.0 V where H_2 would evolve, because the production of H_2 plays an important role in the generation of atomic H* [8,19,39]. In this case, however, with a low applied cathode potential (i.e. −0.5 V), the highest eletroreduction efficiency can be achieved without H_2 evolution. Therefore, it is rationally deduced that rGO sheets as the supporting material loaded Pd nanoparticles play a key role in the electroreduction of H_2O/H^+ to produce atomic H*, thus facilitating the indirect reduction of BrO_3^- to Br^-. The

main reactions involved in the indirect process can be expressed as follows:

$$Pd + H_2O + e^- \rightarrow Pd - H^* + OH^-/Pd + H^+ + e^- \rightarrow Pd - H^* \quad (1)$$

$$6Pd - H^* + BrO_3^- \rightarrow 6Pd + Br^- + 3H_2O \quad (2)$$

$$2Pd - H^* \rightarrow 2Pd + H_2 \quad (3)$$

$$Pd - H^* + H^+ + e^- \rightarrow Pd + H_2 \quad (4)$$

The indirect hydrodeoxygenation on Pd-loaded electrodes proceeds primarily via reaction 1 and 2, with reaction 1 being the rate-limiting step. Decreasing potentials from 0 to −0.5 V exponentially increase the rate of the electron-transfer reaction 1, as well as that of corresponding reaction 2 due to the sufficiently generated atomic H*. Accordingly, the rate constant *k* increases successively until the saturation of atomic H* on the cathode surface is achieved at −0.5 V. Moreover, further decrease of the cathode potentials should lead to faster rate of reaction 3 and 4, especially when the potential is set more negative than that for H_2 evolution, which can explain the negligible decrement in the catalytic efficiency. It is interesting to note that at 0 V, the BrO_3^- content is found to remain nearly constant without the generation of Br^- on the rGO/C electrode; meanwhile, 7.3% of BrO_3^- is reduced to the identical amount of Br^- on the Pd/rGO/CFP electrode. These results indicate that no adsorption effect of BrO_3^- contributes to its catalytic reduction with the composite film cathode, on which the slight BrO_3^- removal in the absence of applied potential may arise from electron transfer between the rGO support and electron-deficient sites on the fine Pd nanoparticles [40].

3.4. Effect of solution pH

A comparison of BrO_3^- reduction at −0.5 and −1.5 V with various pH values was performed in order to explore the role of H^+ in the indirect reduction process on the Pd/rGO/CFP electrode (Fig. 5). The rate constant of BrO_3^- removal is significantly increased from 0.059 to 0.149 min^{-1} upon decreasing pH from 8.07 to 2.10 at −0.5 V. While at −1.5 V, the rate constant *k* is slightly increased from 0.085 to 0.113 min^{-1} when the pH decreases from 8.03 to 4.02, and instead is decreased to 0.082 min^{-1} at pH 2.07. At −0.5 V, the initial concentration of H^+ increased with the drop in pH, contributing to the accumulation of more atomic H* through reaction 1. Therefore, the dramatically increased rate constant at low pH verifies the predominant contribution of atomic H* derived from H_2O/H^+ to BrO_3^- removal with a low potential. It should be noted that at the potential of −1.5 V, H_2 evolution occurs obviously; reaction 4 becomes increasingly important with decreasing pH values. Nevertheless, the evolution of H_2 does not preclude saturation of the atomic H* reduction mechanism for BrO_3^-, since not all the atomic H* may be accessible by BrO_3^- [16]. Therefore, the electroreduction can still be enhanced when surface coverage of adsorbed atomic H* increases with lowering pH values, until the vigorously bubbled H_2 turns to be a barrier suppressing BrO_3^- reduction at pH 2.07. As mentioned above, there are two sources for atomic H*, (1) electroreduction of H_2O/H^+ on polarized Pd particles and (2) activation of H_2. Pathway 1 is dominant at a less negative potential. By contrast, the two pathways simultaneously contribute to the electroreduction at the potential more negative than −1.0 V, leading to the relatively weak pH effect.

3.5. Effect of GO concentration

The performance of the Pd/rGO/CFP electrode is also evaluated by controlling the concentration of GO precursor (C_{GO}) and the results are shown in Fig. S3. When C_{GO} is increased from 0.5 to 1.0 or 1.5 mg/mL, the rate constant is found to be 0.104, 0.110 and 0.105 min^{-1}, respectively, reflecting a negligible effect of C_{GO} on BrO_3^- reduction. However, as C_{GO} is further increased to 2.0 mg/mL, a sufficient amount of rGO is formed to fully cover the carbon fibers with the rate constant increasing to be 0.176 min^{-1}. The obtained results above indicate the high and stable electrocatalytic activity of the Pd/rGO/CFP electrode prepared by reducing GO dispersions with a wide range of concentrations.

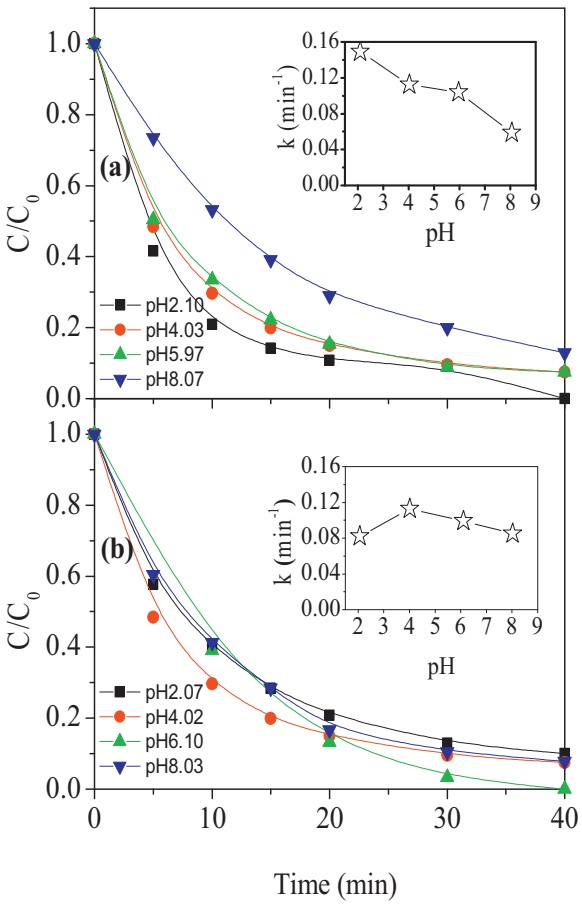

Fig. 5. Effect of solution pH on BrO_3^- reduction at (a) −0.5 V and (b) −1.5 V on the Pd/rGO/CFP electrode (initial BrO_3^- concentration: 1 mg/L, 2 mM Na_2SO_4, GO = 1.5 mg/mL).

3.6. Electrochemical analysis

CV and EIS are typical methods for evaluating the rate of electron transfer on carbon materials-based electrodes. As shown in Fig. 6a, the current density obtained with the Pd/rGO/CFP electrode is substantially higher in the potential range from 0 to −1.5 V, in comparison with that of CFP, rGO/CFP and Pd/CFP electrode. The onset potential of the Pd/rGO/CFP electrode is around −0.3 V, more positive than that obtained at the other three electrodes, indicating that the BrO_3^- reduction is more kinetically favorable at the composite film electrode. In EIS, the semicircle portion observed at high frequencies corresponds to the electron transfer limiting process (Fig. 6b). The dramatically decreased semicircle of the Pd/rGO/CFP reveals that the rapid electron transfer between BrO_3^- and the composite film electrode could be achieved. As reported by Li et al., graphene sheets can offer substantial benefits with regard to mass transfer and charge transport, by providing shorter effective lengths for both electronic and ionic

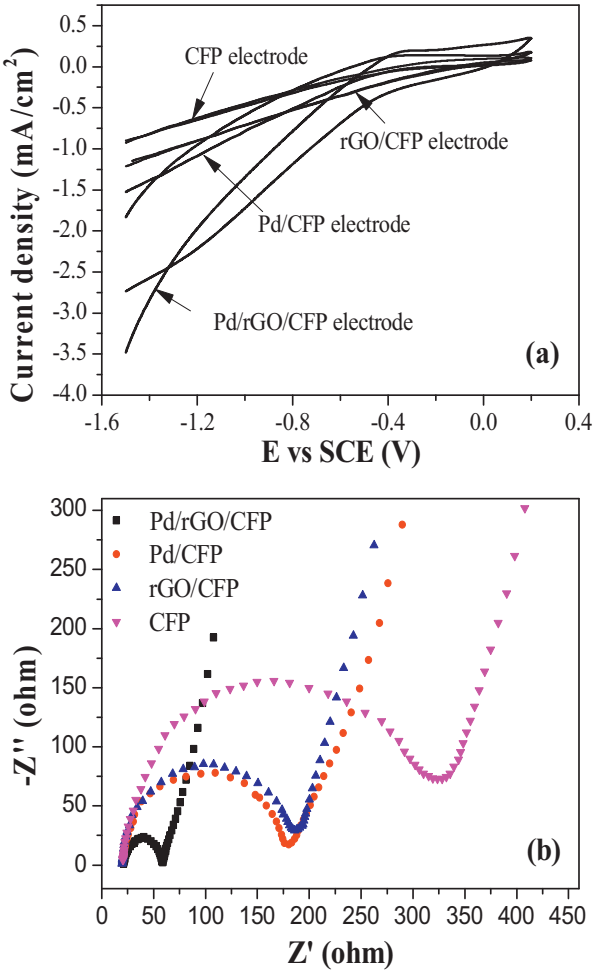

Fig. 6. (a) CV display of the electrodes in 2 mM Na_2SO_4 and 1 mM BrO_3^- (scan rate: 50 mV/s). (b) Nyquist diagrams obtained at the electrodes in 2 mM Na_2SO_4 and 1 mM BrO_3^-.

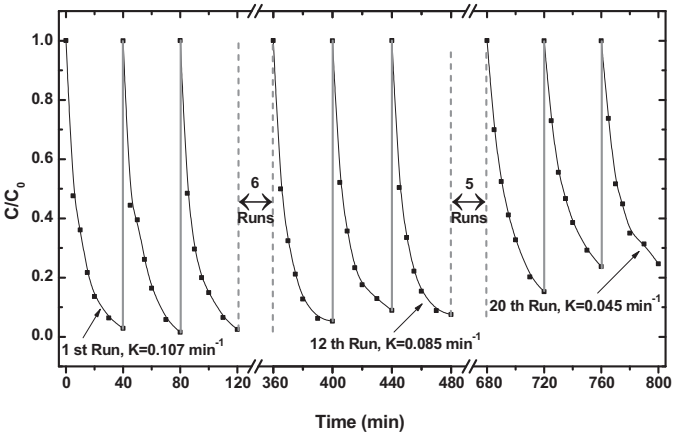

Fig. 7. Repeated reduction of BrO_3^- at the Pd/rGO/CFP electrode (initial BrO_3^- concentration: 1 mg/L, applied bias potential: −0.5 V, 2 mM Na_2SO_4, pH = 6.03). The same cathode was used for 20 successively repeated applications.

transport [21]. Herein, the rGO nanosheets-coated CFP is believed to possess multifunctional roles in facilitating the dispersion of metallic Pd clusters and charge transfer due to its unique electronic structure and abundance of surface defects (such as kinks, surface oxides, etc.). With the collaborative effects including the enhanced electron mobility that stems from rGO nanosheets and the unique property for production of atomic H* due to the Pd nanocrystals, the Pd/rGO/CFP electrode exhibits the highest catalytic activity and electrical conductivity as compared to other electrodes.

Combined with the results of BrO_3^- electroreduction, it can be concluded that the Pd/rGO/CFP electrode can offer more active sites that are accessible for transformation of H_2O/H^+ to atomic H* than the individual Pd/CFP electrode. Particularly, at low cathode potentials, reaction 1 with a relatively slow rate on the Pd/CFP electrode may not be able to generate sufficient atomic H* for BrO_3^- reduction. In contrast, the rGO sheets of the composite film electrode can play an effective role in accelerating the electroreduction of H_2O/H^+ on the polarized Pd particles, so reactions (1) and (2) can be carried out adequately. Additionally, it is worth mentioning that the cathode potential required for the complete reduction of BrO_3^- to Br^- on the Pd/rGO/CFP electrode could be as low as -0.5 V, less negative than the overpotential for H_2 evolution. That means the removal of BrO_3^- could be achieved on our composite film electrode without the side reaction of H_2 evolution, which occurred frequently in the Pd-catalytic eletroreduction processes [8,9,15].

3.7. Long-term performance

The stability of the Pd/rGO/CFP electrode is further evaluated by batch reduction experiments. As shown in Fig. 7, the efficiency maintains almost constant from the first to the tenth applications, and gradually decreases afterwards. Although the rate constant k decreases to be 0.085 min^{-1} in the twelfth application, the removal efficiency is observed to be as high as 92.6%, suggesting a long-lasting electrocatalytic activity of the Pd/rGO/CFP electrode.

XRD patterns and SEM image (Fig. 8a) reveal that for the used Pd/rGO/CFP electrode, Pd with sphere-like nanoclusters had transformed into star-like nanoclusters over the rGO sheets that consist of several nanotips, with the primary crystallite size increasing to be 16.7 nm. According to the perturbation theory, the adsorption of H may displace the Pd atom from its initial location on the supporting rGO sheets [41]. The displacement is rooted on the fact that the Pd—H interaction is as strong as the Pd—C interaction. The observed restructuring of the Pd facets can thus be attributed to that their interactions also occur for larger Pd clusters during the BrO_3^- reduction process, leading to the "stars" perpendicular to the rGO support, as well as the increased Pd crystallite size. This change decreases the surface reactive sites on the Pd/rGO/CFP cathode. XPS results in Fig. 8b and c indicate that rGO sheets are not altered fundamentally after 20 repeated reduction treatments. PdO_x species on the used Pd/rGO/CFP electrode disappear, which may be caused by the electroreduction of PdO_x at the cathode. And, metallic Pd^0 is observed with nearly no loss in the peak intensities. As a result, the good stability of the Pd/rGO/CFP electrode is attributed to that the Pd nanoparticles can stably adhere on the uniform rGO sheets for a long time due to their strong interactions. The increased primary Pd crystallite size on the rGO sheets not only reduces particle surface area, but also decreases the fractions of more reactive surface Pd atoms such as those on edge and vertex sites, leading to the slightly declined activity with durations [42]. Further investigations could be focused on the combination of Pd and other metals as to fabricate bimetallic or trimetallic surfaces, which may serve to mitigate the effect of Pd—H interaction on the Pd dispersions.

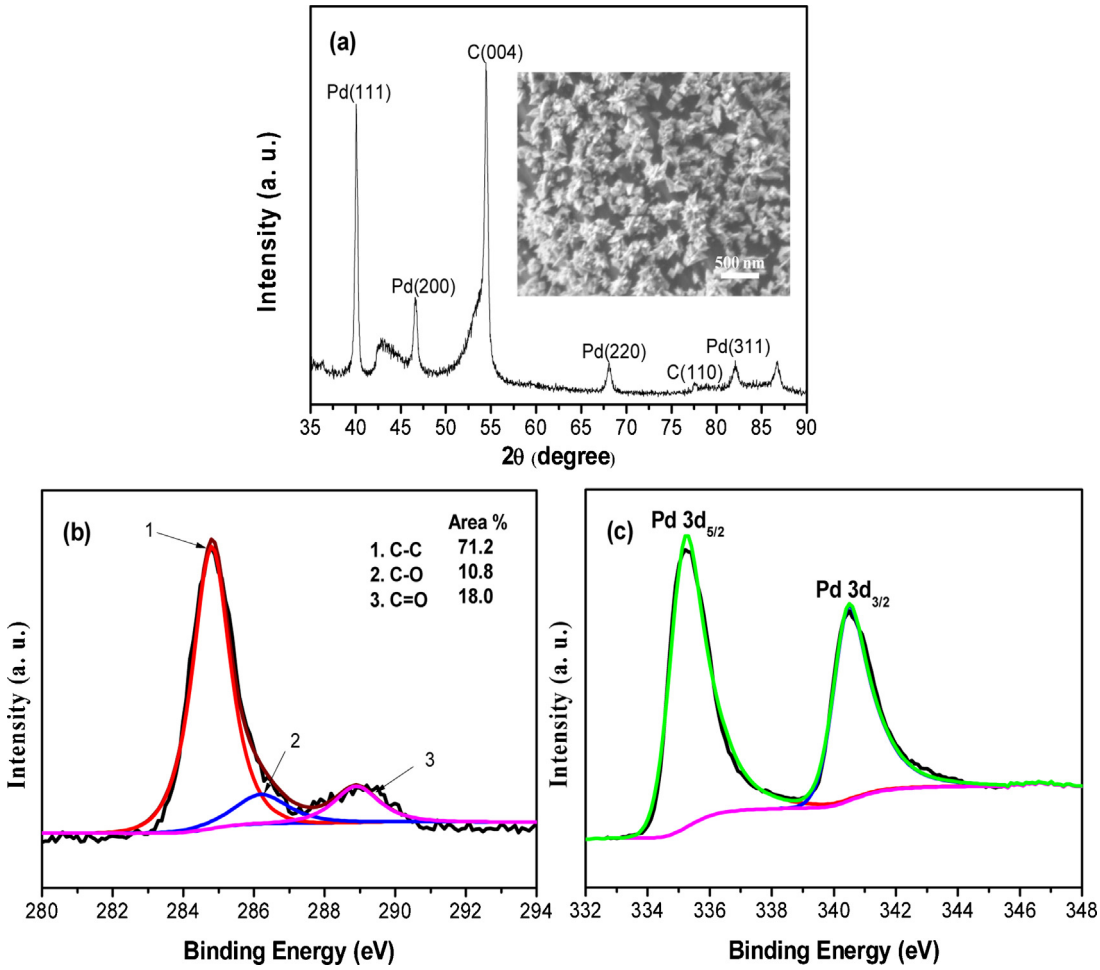

Fig. 8. (a) XRD patterns, (b) XPS C 1s spectrum and (c) XPS Pd 3d spectrum of the Pd/rGO/CFP electrode after 20 successively repeated applications, inset is the SEM image of the same electrode.

4. Conclusions

A novel composite film cathode, Pd/rGO/CFP, is synthesized via green chemical reduction of the GO film on the CFP substrate, followed by electrochemically depositing Pd nanoparticles. The Pd/rGO/CFP electrode shows higher electrocatalytic activity in the BrO_3^- electroreduction than CFP, Pd/CFP and rGO/CFP electrode. In the cathode potential range from 0 to −2.0 V, the highest BrO_3^- reduction rate can be achieved at −0.5 V, without the side reaction of H_2 evolution. The strong pH dependence at −0.5 V verifies the predominant contribution of atomic H* derived from H_2O/H^+ to BrO_3^- removal; the weaker pH effect at −1.5 V indicates that the activation of H_2 turns to be another source for atomic H* production. CV and EIS analysis further demonstrates the collaborative effects of the rGO nanosheets and Pd nanocrystals on the indirect BrO_3^- reduction. Pd—H interaction in the indirect reduction process may result in the displacement of Pd nanoparticles, thus leading to the slightly declined activity with repeated treatments.

Acknowledgments

This work was supported by National Natural Science Foundation of China (No. 51290282, 51222802, 51221892) and State Key Development Program of Basic Research of China (No. 2010CB933604).

Appendix A. Supplementary data

Supplementary data associated with this article can be found, in the online version, at http://dx.doi.org/10.1016/j.apcatb.2014.04.040.

References

[1] H.S. Weinberg, C.A. Delcomyn, V. Unnam, Environ. Sci. Technol. 37 (2003) 3104–3110.
[2] K. Listiarini, J.T. Tor, D.D. Sun, J.O. Leckie, J. Membr. Sci. 365 (2010) 154–159.
[3] T.Y. Li, Y.M. Chen, P.Y. Wan, M.H. Fan, X.J. Yang, J. Am. Chem. Soc. 132 (2010) 2500–2501.
[4] M.J. Kirisits, V.L. Snoeyink, H. Inan, J.C. Chee-Sanford, L. Raskin, J.C. Brown, Water Res. 35 (2001) 891–900.
[5] J. Liu, J.W. Yu, D. Li, Y. Zhang, M. Yang, Biochem. Eng. J. 65 (2012) 44–50.
[6] R. Butler, A. Godley, L. Lytton, E. Cartmell, Crit. Rev. Env. Sci. Technol. 35 (2005) 193–217.
[7] M.A. Hasnat, M. Saiful Alam, M.H. Mahbub-ul Karim, M.A. Rashed, M. Machida, Appl. Catal., B: Environ. 107 (2011) 294–301.
[8] W. Xie, S. Yuan, X. Mao, W. Hu, P. Liao, M. Tong, A.N. Alshawabkeh, Water Res. 47 (2013) 3573–3582.
[9] B. Yang, G. Yu, J. Huang, Environ. Sci. Technol. 41 (2007) 7503–7508.
[10] L. Ding, Q. Li, H. Cui, R. Tang, H. Xu, X.C. Xie, J.P. Zhai, Electrochim. Acta 55 (2010) 8471–8475.
[11] J. Radjenovic, M.J. Farre, Y. Mu, W. Gernjak, J. Keller, Water Res. 46 (2012) 1705–1714.
[12] N. Kishimoto, N. Matsuda, Environ. Sci. Technol. 43 (2009) 2054–2059.
[13] X. Zhao, H.J. Liu, A.Z. Li, Y.L. Shen, J.H. Qu, Electrochim. Acta 62 (2012) 181–184.
[14] T. Li, J. Farrell, Environ. Sci. Technol. 34 (2000) 173–179.
[15] S.H. Yuan, X.H. Mao, A.N. Alshawabkeh, Environ. Sci. Technol. 46 (2012) 3398–3405.
[16] J.K. Wang, J. Farrell, Environ. Sci. Technol. 37 (2003) 3891–3896.

[17] B.P. Chaplin, M. Reinhard, W.F. Schneider, C. Schüth, J.R. Shapley, T.J. Strathmann, C.J. Werth, Environ. Sci. Technol. 46 (2012) 11469–11470.
[18] W.C. Conner, J.L. Falconer, Chem. Rev. 95 (1995) 759–788.
[19] A.Z. Li, X. Zhao, Y.N. Hou, H.J. Liu, L.Y. Wu, J.H. Qu, Appl. Catal., B: Environ. 111–112 (2012) 628–635.
[20] M.J. Allen, V.C. Tung, R.B. Kaner, Chem. Rev. 110 (2009) 132–145.
[21] Y.M. Li, L.H. Tang, J.H. Li, Electrochem. Commun. 11 (2009) 846–849.
[22] D. Kim, M.S. Ahmed, S. Jeon, J. Mater. Chem. 22 (2012) 16353–16360.
[23] L.H. Tang, Y. Wang, Y.M. Li, H.B. Feng, J. Liu, J.H. Li, Adv. Funct. Mater. 19 (2009) 2782–2789.
[24] Y.G. Kim, Z.A. Akbar, D.Y. Kim, S.M. Jo, S.Y. Jang, ACS Appl. Mater. Interfaces 5 (2013) 2053–2061.
[25] M.Y. Yen, C.C. Teng, M.C. Hsiao, P.I. Liu, W.P. Chuang, C.C.M. Ma, C.K. Hsieh, M.C. Tsai, C.H. Tsai, J. Mater. Chem. 21 (2011) 12880–12888.
[26] V. Sridhar, H.J. Kim, J.H. Jung, C.G. Lee, S.J. Park, I.K. Oh, ACS Nano 6 (2012) 10562–10570.
[27] X.M. Chen, G.H. Wu, J.M. Chen, X. Chen, Z.X. Xie, X.R. Wang, J. Am. Chem. Soc. 133 (2011) 3693–3695.
[28] C.C. Huang, C. Li, G.Q. Shi, Energy Environ. Sci. 5 (2012) 8848–8868.
[29] M. Segal, Nat. Nanotechnol. 4 (2009) 611–613.
[30] M. Zhang, D.B. Bacik, C.B. Roberts, D.Y. Zhao, Water Res. 47 (2013) 3706–3715.
[31] H.L. Wang, J.T. Robinson, X.L. Li, H.J. Dai, J. Am. Chem. Soc. 131 (2009) 9910–9911.
[32] A. Gupta, G. Chen, P. Joshi, S. Tadigadapa, P.C. Eklund, Nano Lett. 6 (2006) 2667–2673.
[33] H.C. Choi, M. Shim, S. Bangsaruntip, H.J. Dai, J. Am. Chem. Soc. 124 (2002) 9058–9059.
[34] J.Y. Qu, X.Q. Zou, B.F. Liu, S.J. Dong, Anal. Chim. Acta 599 (2007) 51–57.
[35] J. Farrell, N. Melitas, M. Kason, T. Li, Environ. Sci. Technol. 34 (2000) 2549–2556.
[36] L.E. Knitt, J.R. Shapley, T.J. Strathmann, Environ. Sci. Technol. 42 (2008) 577–583.
[37] D. Shuai, B.P. Chaplin, J.R. Shapley, N.P. Menendez, D.C. McCalman, W.F. Schneider, C.J. Werth, Environ. Sci. Technol. 44 (2010) 1773–1779.
[38] I.F. Cheng, Q. Fernando, N. Korte, Environ. Sci. Technol. 31 (1997) 1074–1078.
[39] Y.P. Li, H.B. Cao, Y. Zhang, Water Res. 41 (2007) 197–205.
[40] S. Gomez-Quero, F. Cardenas-Lizana, M.A. Keane, Ind. Eng. Chem. Res. 47 (2008) 6841–6853.
[41] I. Cabria, M.J. Lopez, S. Fraile, J.A. Alonso, J. Phys. Chem. C 116 (2012) 21179–21189.
[42] J.C. Liu, F. He, E. Durham, D.Y. Zhao, C.B. Roberts, Langmuir 24 (2008) 328–336.